Supporting Information for "Anthropogenic aerosols have significantly weakened the regional summertime circulation in the Northern Hemisphere during the satellite era"

Joonsuk M. Kang[1], Tiffany A. Shaw[1], Lantao Sun[2]

[1]Department of the Geophysical Sciences, The University of Chicago, Chicago, IL, 60637

[2]Department of Atmospheric Sciences, Colorado State University, Fort Collins, CO, 80521

Contents of this file

1. Tables S1
2. Figures S1 to S11

Introduction

This document includes supporting information for the main text (1 table and 11 figures).

References

Henley, B. J., Gergis, J., Karoly, D. J., Power, S., Kennedy, J., & Folland, C. K. (2015). A tripole index for the interdecadal Pacific oscillation. *Climate dynamics*, *45*, 3077–3090.

Table S1. Number of realizations used from each model to calculate different storm track metrics and MSE budget.

Models	EKE	ECA	MSE budget
ACCESS-CM2	0	3	3
ACCESS-ESM1-5	3	3	0
CanESM5	9	10	10
CNRM-CM6-1	3	3	0
FGOALS-g3	1	2	3
GFDL-ESM4	0	1	0
HadGEM3-GC31-LL	5	5	5
IPSL-CM6A-LR	6	5	0
MIROC6	3	3	3
MRI-ESM2-0	5	5	5
NorESM2-LM	0	3	0
Total	35	43	26

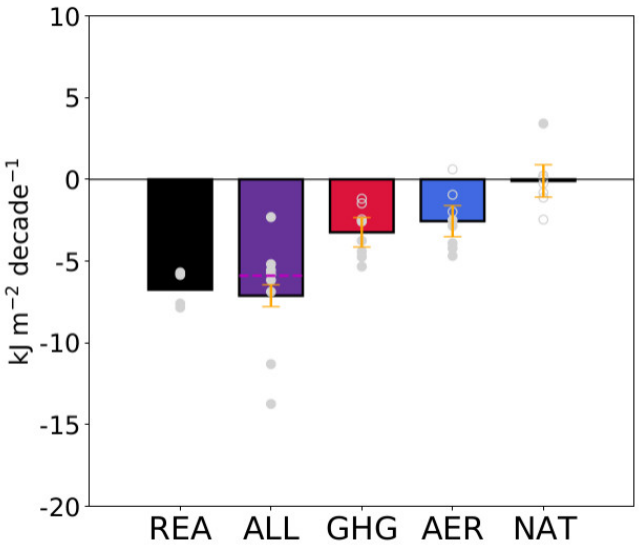

Figure S1. Similar results to Fig. 1d, but circles show trends averaged across different realizations in 8 models.

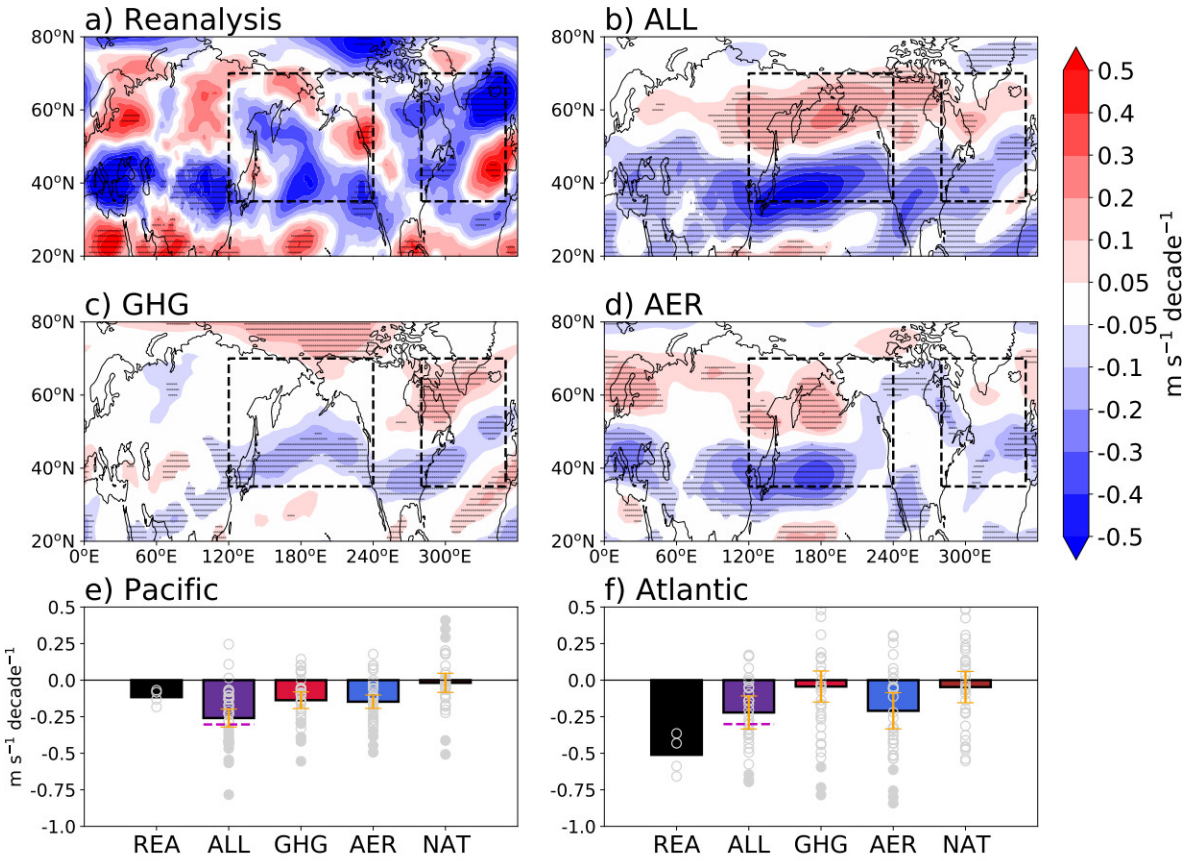

Figure S2. Similar results to Fig. 2, but for U500 trends.

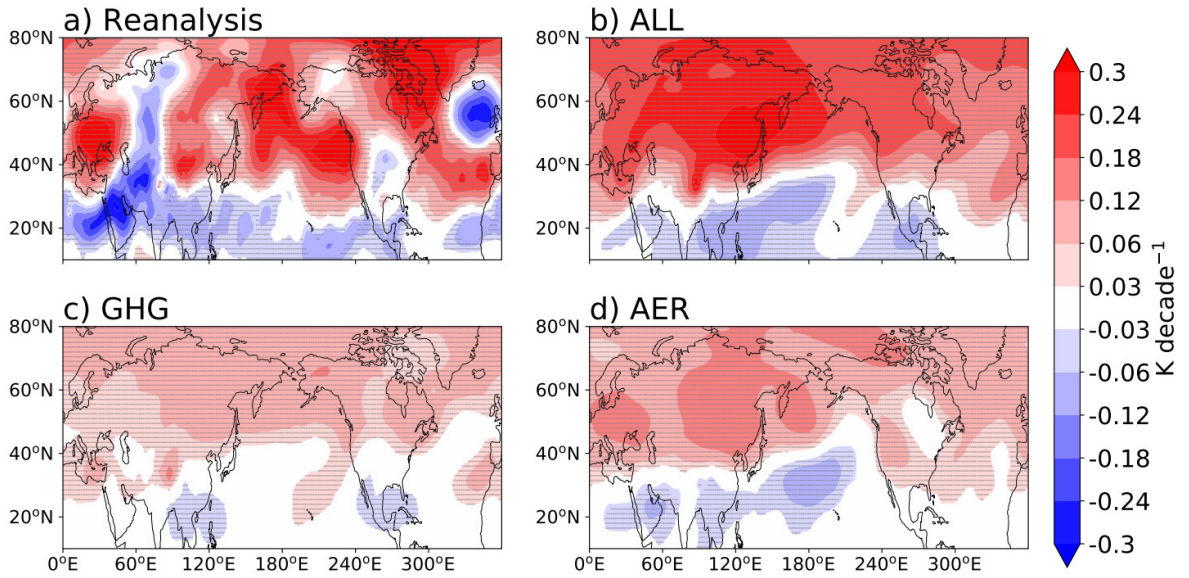

Figure S3. Similar results to Figs. 2a–d, but for 500-hPa temperature trends. Global-mean trend is removed to emphasize the gradients

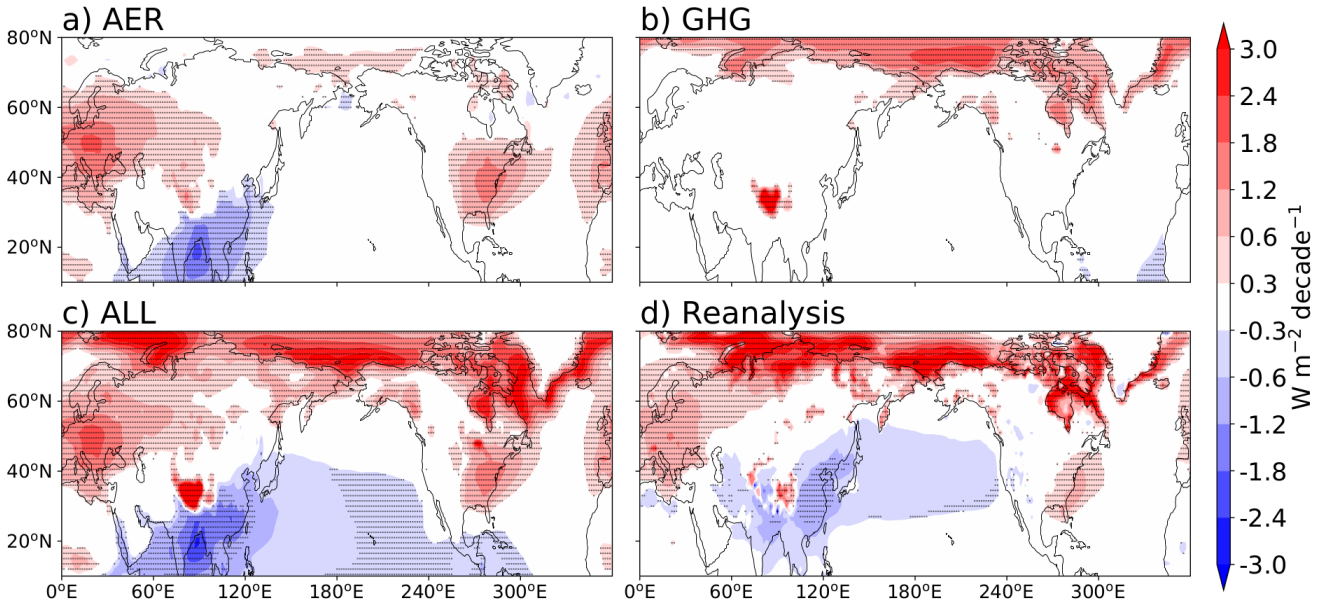

Figure S4. Similar results to Fig. 4, but for clear-sky shortwave radiation at the top of the atmosphere.

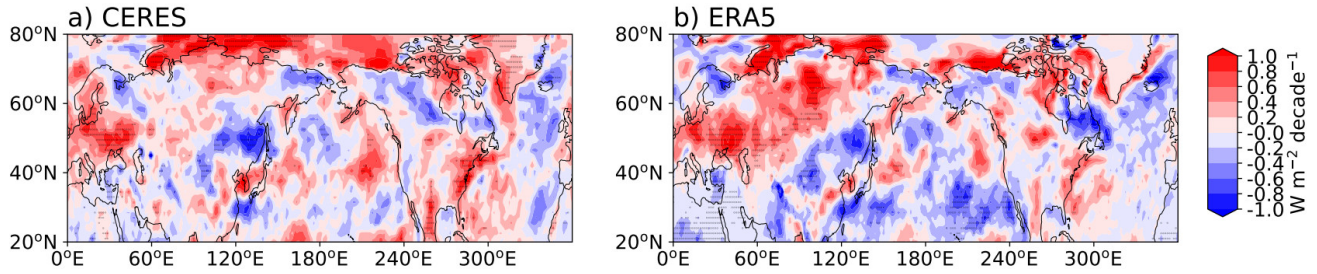

Figure S5. Spatial pattern of JJA top-of-atmosphere shortwave radiation trends from 2000 to 2020 in (a) CERES and (b) ERA5. Statistically significant trends at the 95% confidence level are stippled.

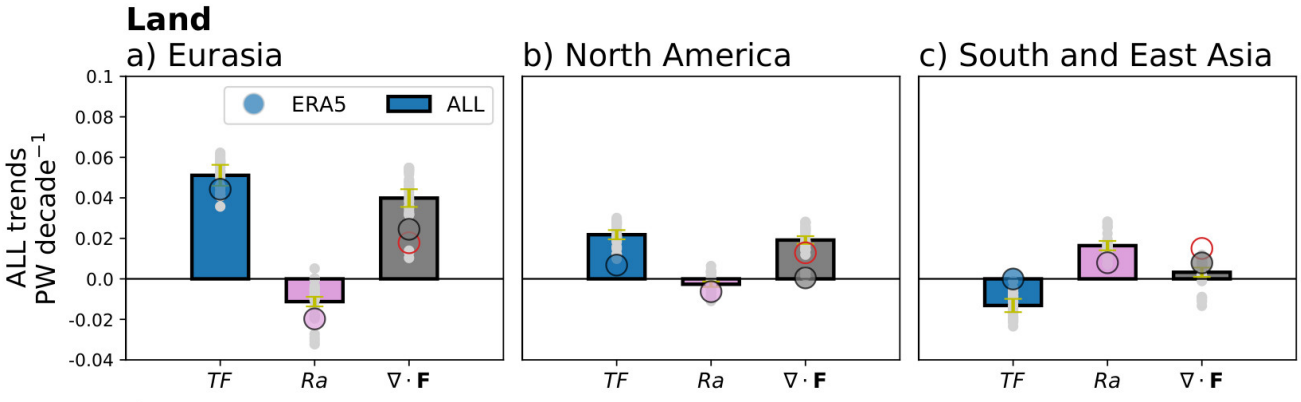

Figure S6. (a) Linear trends in surface turbulent flux (blue), radiative cooling (pink), and MSE flux divergence (gray) from 1980 to 2020 in ERA5 (circles) and ALL simulations (bars: ensemble mean, dots: ensemble members) over Eurasia domain in Fig. 7. (b, c) Same as (a), but for (b) North America and (c) South and East Asia. Red circles represent MSE flux divergence trends due to stationary circulations ($\nabla \cdot \mathbf{F_{SC}}$).

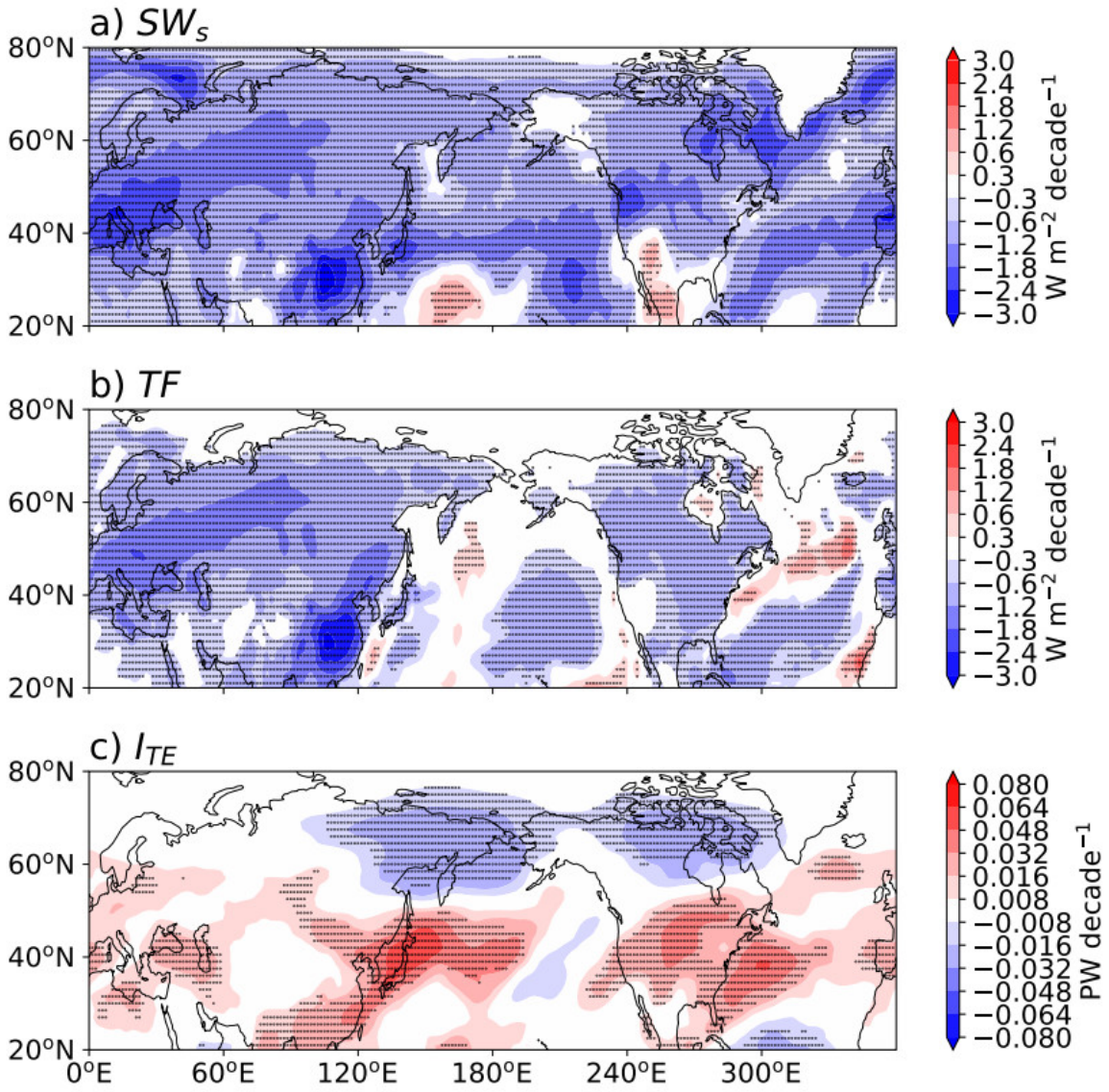

Figure S7. Spatial structure of JJA ensemble-mean trends from 1940 to 1980 of (a) surface shortwave radiation, (b) surface turbulent fluxes, and (c) storm track intensity in the AER simulations. Statistically significant trends at the 95% confidence level are stippled.

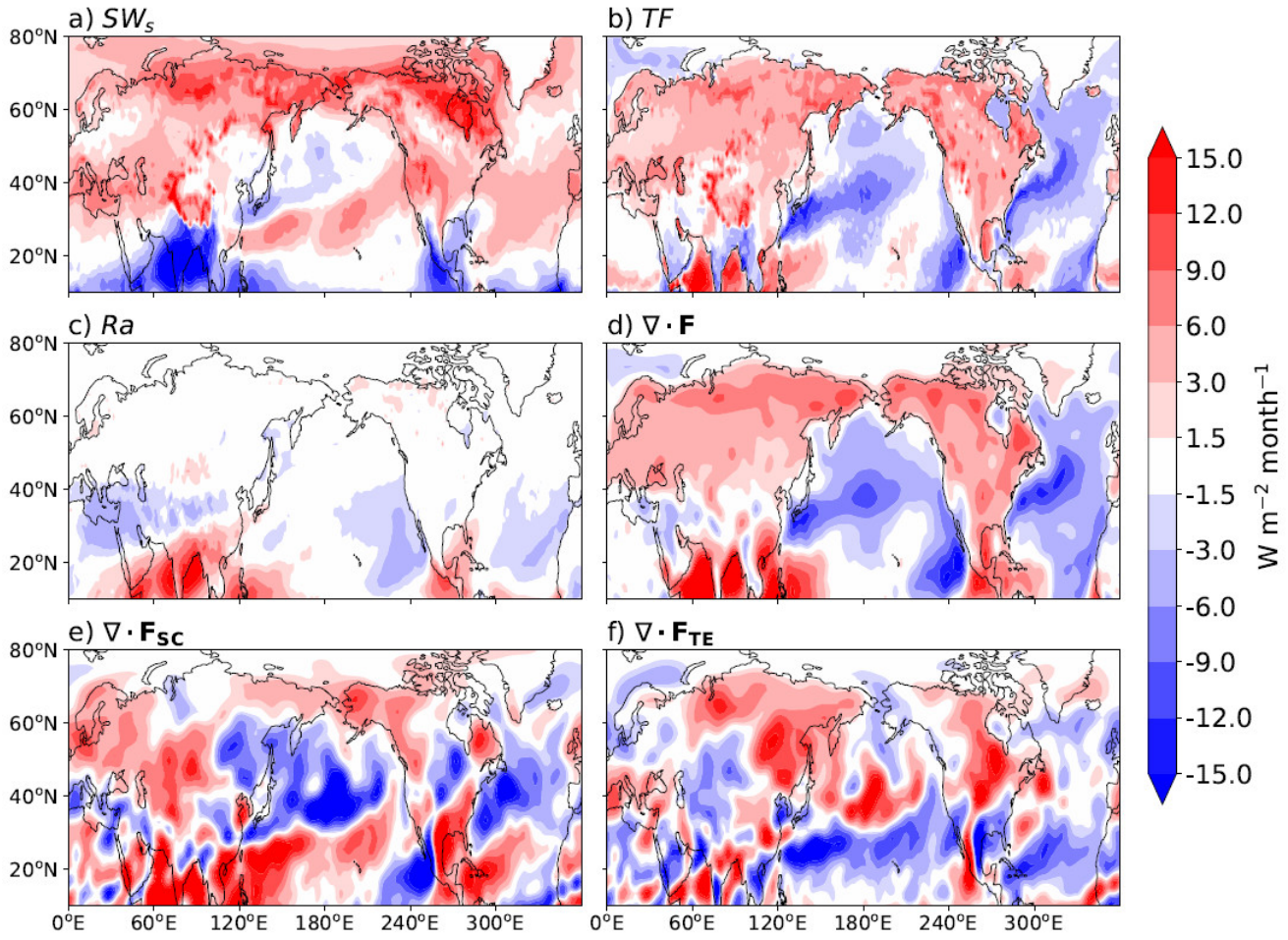

Figure S8. Similar results to Fig. 5, but during climatological seasonal transition from spring to summer (June minus May) in ERA5.

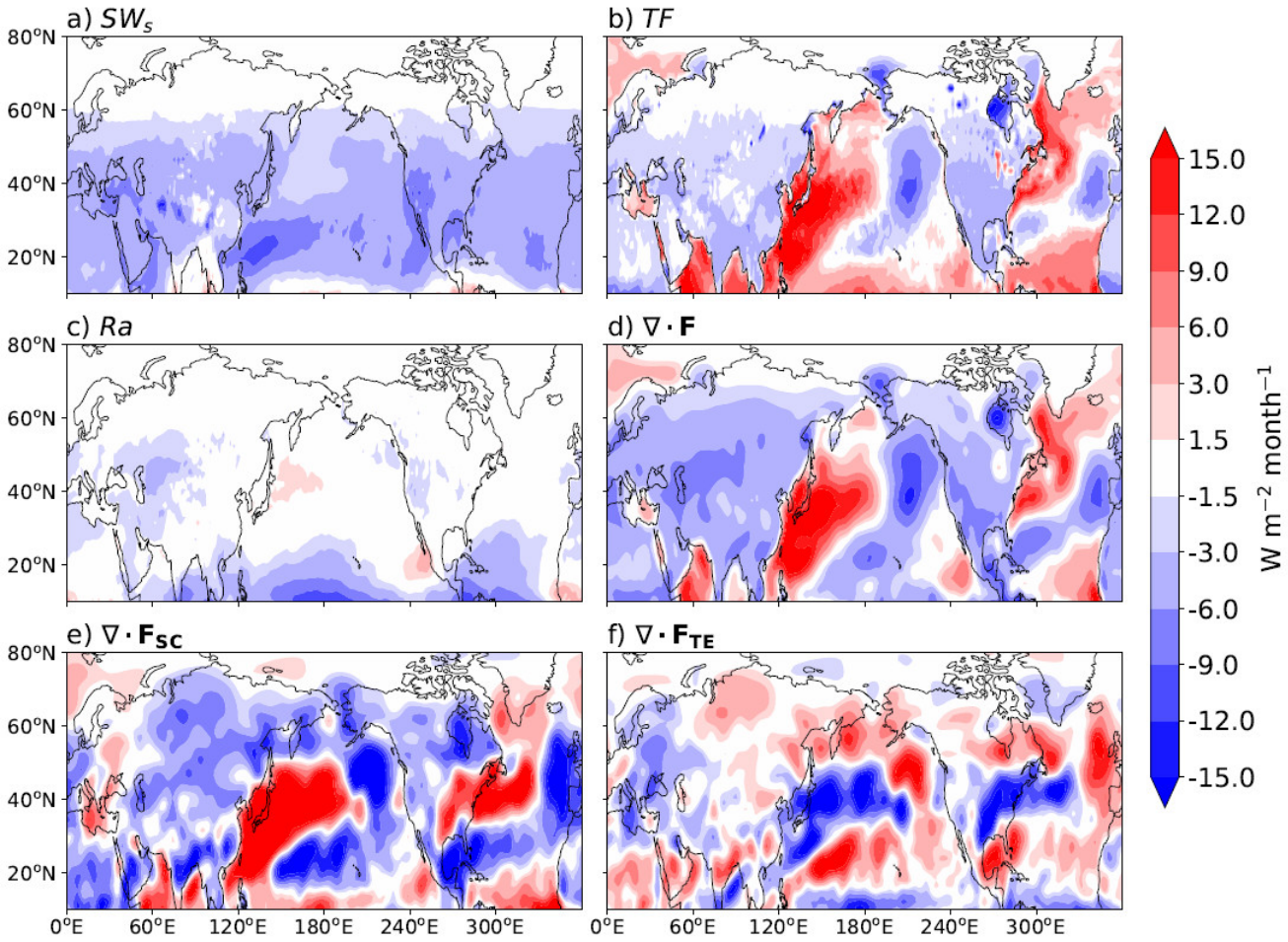

Figure S9. Similar results to Fig. 5, but during climatological seasonal transition from fall to winter (December minus November) in ERA5.

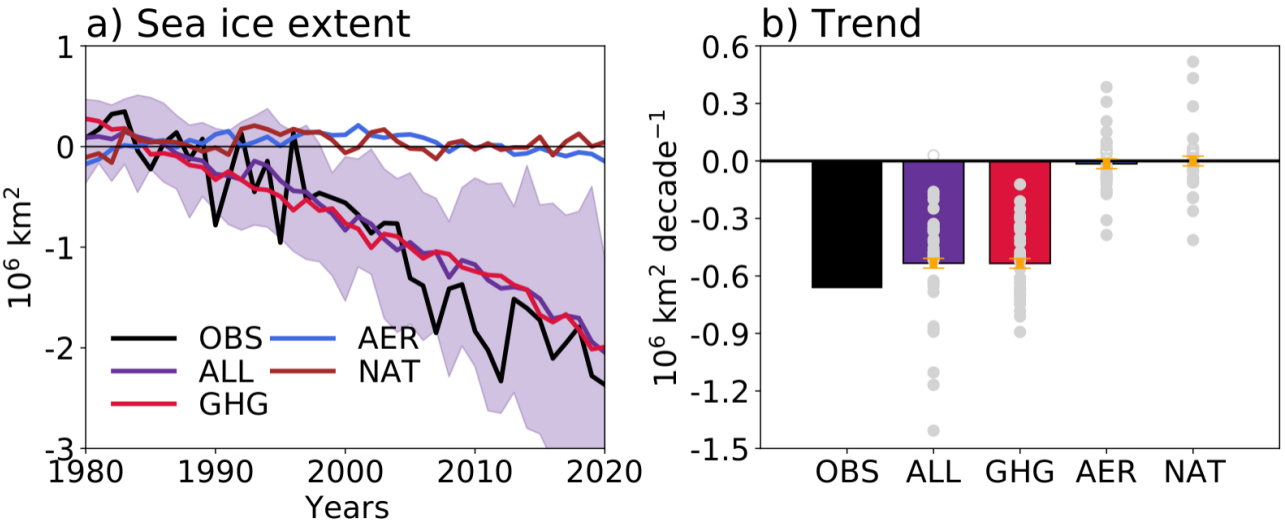

Figure S10. Similar results to Fig. 1, but for JJA Arctic sea ice extent defined as area containing sea ice fraction greater than 15%. The observed sea ice extent is obtained from the National Snow and Ice Data Center (`https://nsidc.org/home`).

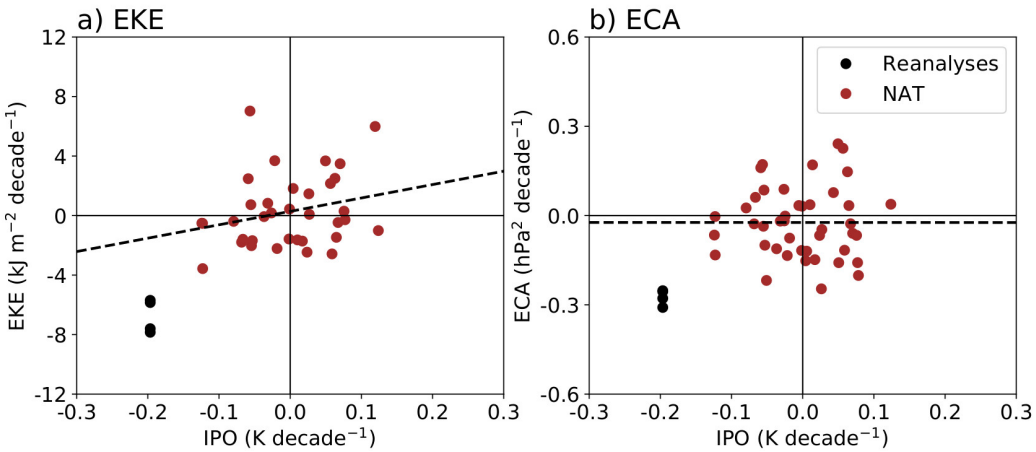

Figure S11. (a) Scatter plot of IPO (x-axis) and NH JJA EKE (y-axis) trends from 1980 to 2020 in (black) reanalyses and (purple) NAT simulations. (b) Similar results to (a), but for ECA trends. The IPO trends are calculated following (Henley et al., 2015).